Kinetic modelling of combustion in a spark ignition engine with water injection

Hao Yuan[a,*], Karl Giles[a], Sipeng Zhu[a], Simeon Howson[a] , Andrew Lewis[a] , Sam Akehurst[a] , Niall Turner[b], James Harris[b], Gavin Fowler[b], John Geddes[b]

[a]*Department of Mechanical Engineering, University of Bath, Bath BA2 7AY, United Kingdom*

[b]*Jaguar Land Rover, Coventry CV3 4LF, United Kingdom*

Abstract

This work models the impact of direct water injection on the combustion process in a spark ignition engine. It uses a two-zone kinetic model coupled with detailed combustion chemistry to highlight the thermodynamic and chemical-kinetic interactions between gasoline combustion and water injection. The modelling results agree closely with measurements from a highly boosted, direct injection gasoline engine.

This study first proposes an approach to model the mass fraction burned (MFB) profile using a representative in-cylinder pressure trace. The derived MFB profile is then used as the input for a two-zone kinetic model. Within this model, predictive kinetic modelling is used to estimate the knock limited spark advance (KLSA) for a baseline engine operating condition without water injection and subsequently, for several conditions with water injection. Predicted KLSA values obtained using this method agree closely with measured results.

Utilising the approach developed in this study, the modelled MFB profile at the baseline operating condition was found to be similar to that obtained at the condition with a water/fuel ratio (WFR) of 60%. This result is likely due to the competing and contrasting effects of reduced in-cylinder temperature versus more advanced combustion phasing at conditions with water injection. Further thermodynamic analysis shows that the charge cooling effect afforded by direct water injection is much greater than the dilution effect in terms of advancing the knock limited combustion phasing. Water injection also affects the kinetic processes that take place in the unburned gas zone, but mainly by altering the in-cylinder thermodynamic conditions – the injected water is not directly involved in the low temperature chemistry in the unburned gas zone, it simply acts as a collision partner.

*Corresponding author:
Email address: yuanhaoars@gmail.com h.yuan@bath.ac.uk (Hao Yuan)

Keywords: Kinetic Model, Engine Combustion, Water Injection, Spark Ignition

1. Introduction

The increasingly stringent requirements of new and upcoming emissions legislation (e.g. EURO 6d standards and China 6 regulations) have led to the wide application of highly boosted, downsized, and direct injected (DI) spark ignition (SI) engines. However, the combination of high pressures and temperatures inside the combustion chambers of modern SI engines makes knocking combustion more likely to occur, limiting engine performance and efficiency. One approach that that has been employed in recent years to resolve this issue has been to blend alcohols into commercial gasolines, thus utilising the charge cooling effects and the high octane numbers of alcohols to mitigate knock [1–4]. More recently, water injection has been considered as a promising technology to achieve the same objective but at reduced environmental impact. Moreover, future emissions regulations such as EU7 and the adoption of Real Driving Emissions testing (which excite more of the engine operating envelope) are likely to prevent the use of fuel-enrichment for exhaust gas temperature control in gasoline engines due to strict limits on carbon monoxide and total hydrocarbon emissions. With water's high heat of vaporisation and high specific heat capacity, water injection is considered to be a potential candidate technology to enable whole-map stoichiometric operation and thereby comply with future emissions regulations.

Both experimental and numerical studies have been performed to investigate the impact of water injection on engine performance. A detailed review of applying water injection in combustion engines was performed by Zhu et al. [5]. Therefore, this study only provides a brief review of the recent application of water injection in SI engines. In the 1980s, Harrington [6] carried out engine experiments to study water addition on gasoline engines and found that water addition extends the knock limited spark advance, decreases nitric oxide (NO) emissions, slightly increases unburned hydrocarbon emissions, and has little effect on carbon monoxide (CO) emissions. Recent experimental studies [7–12] confirmed the findings of Harrington [6] in modern spark ignition engines with either port fuel injection (PFI) or DI. Numerical studies employing 1D thermodynamic modelling [13,14] and 2D/3D computational fluid dynamics (CFD) modelling [15–18] techniques have also been performed to understand the

impact of water injection on the combustion phasing and to optimize experimental conditions. These experimental and numerical studies found that water injection improves engine efficiency by enabling a more advanced spark timing due to the charge cooling effect, and, not surprisingly, the improvement is more pronounced with direct water injection. The lower peak temperature afforded by water injection were also found to inhibit the formation of nitrogen oxides (NOx). However, emissions of unburned hydrocarbons were found to increase as a result of water injection since the charge cooling effect may introduce a high level of inhomogeneity (particularly within the crevice volumes) which is likely to trap more fuel. In general, the existing studies mainly focus on the thermodynamic effects of water injection, and the chemical interactions between water and fuel under spark ignition engines are rarely reported [5]. Therefore, this work aims to fill this gap in the literature by conducting kinetic modelling of water/fuel interactions with detailed combustion chemistry.

The knowledge of detailed chemistry of water/fuel interactions comes from the experiments performed in fundamental combustion facilities, such as jet-stirred reactors [19,20], a shock tube [21], and rapid compression machines [21,22]. Le Cong and Dagaut [19] conducted jet-stirred reactor experiments to explore the influence of water vapour on the oxidation of hydrogen- and methane-based mixtures at 800-1500 K, 1 atm., and a residence time of 120 ms with equivalence ratios ranging from 0.1 to 1.5. The corresponding kinetic modelling suggested that water vapour decreases the reactivity of fuel mixtures due to its high third body efficiency. More recently, Donohoe et al. [21] studied the impact of dilution with water vapour on the autoignition behaviours of hydrogen, carbon monoxide, methane, syngas, and natural gas mixtures in a rapid compression machine and a shock tube under conditions of interest to gas turbines. The experimental results showed that the chemical effect of the water addition was only observed for the oxidation of neat carbon monoxide as the added water favours the formation of reactive OH radicals, whereas the reactivity of other fuel mixtures is mainly affected by the change of the thermodynamic properties from the water addition. Apart from the studies on the influence of the water addition on gaseous fuels, He et al. [22] investigated the impact of water addition on the oxidation of iso-octane in a rapid compression machine under 943-1027 K, 5.12-23 atm., and equivalence ratios ranging from 0.25 to 1.0. They

found that the reactivity of iso-octane was slightly increased by 3% water addition on a mole basis. A very recent study by Schmitt et al. [20] found no significant differences between the experiments conducted in a jet-stirred reactor with and without water in the low temperature regime. Based on these experimental studies, water is not likely to alter the oxidation pathways of hydrocarbon fuels in the low temperature regime but may affect combustion processes at relatively high temperatures in practical systems, like SI engines. However, little is known about the impact of the water addition on the combustion process in SI engines, since it is difficult to couple chemical kinetics with complicated in-cylinder thermodynamic conditions.

Efforts have been made in the literature to couple detailed fuel chemistry with thermodynamic modelling of spark ignition engines. Szybist and Splitter [23] performed kinetic simulations with the closed homogeneous reactor model in ANSYS Chemkin to investigate the impacts of pressure and temperature on octane sensitivity. Since the closed homogeneous reactor is essentially a single-zone model, it requires empirical pressure-temperature trajectory from the unburned gas zone as the input and assumes adiabatic conditions and a constant volume. These simplifications and assumptions are acceptable when applied to explore the chemical origin of octane sensitivity, but are not sufficient for rigorous simulations of spark ignition engines. To handle the thermodynamics accurately, Agbro et al. [24] applied the stochastic reactor model (SRM) to simulate the kinetic influence of n-butanol blending on the knocking combustion of gasoline and its surrogate. The probability-based SRM can emulate the mixture inhomogeneity and provides the mixing time as an optimizable parameter which helps to reduce the discrepancy between measurements and simulations. However, the differences reported by Agbro et al. [24] are still significant. Compared with the probability-based SRM which allows empirical tuning, GT-Power [25] offers a built-in chemical kinetic model to simulate the autoignition, which was applied by Morganti et al. [26] to study the autoignition of liquefied petroleum gas in a cooperative fuel research (CFR) engine. The modelling results from [26] agree closely with the measured pressure traces, which enables further kinetic analysis. Nevertheless, to the best of the authors' knowledge, the kinetic model incorporated in GT-Power has not been applied to model spark ignition engines fuelled by gasoline, which is probably due to known issues surrounding

GT-Power's ability to handle large chemical mechanisms for gasoline surrogates. The large size of detailed gasoline surrogate mechanisms is not an issue in ANSYS Chemkin. The two-zone kinetic model recently provided by ANSYS Chemkin couples detailed chemistry with thermodynamic modelling of spark ignition engines. DelVescovo et al. [27] applied this model to study pre-spark heat release and autoignition chemistry of iso-octane in a spark ignition engine. Their modelling results suggested that the well-known low temperature chemistry of iso-octane cannot reproduce the measurements. However, the estimations of thermodynamic factors (e.g. mass fraction burned (MFB) profile) in [27] could have been improved by more rigorous thermodynamic analysis, which is likely to have affected their conclusions.

Considering the issues with the existing kinetic modelling of spark ignition engines, it is critical to have a systematic approach which accurately estimates thermodynamic factors and rigorously couples detailed chemistry with thermodynamic models. To meet these requirements, Foong et al. [28,29] developed a two-zone kinetic model coupled with detailed fuel chemistry to study knocking combustion in a CFR engine and used GT-Power to estimate thermodynamic factors as the inputs of the kinetic modelling. Later, Yuan et al. [4] extended the two-zone kinetic model to simulate knock-limited combustion in a single cylinder research engine. The thermodynamic factors required in the two-zone model include initial thermodynamic states and the MFB profile that quantifies the burning rate from the flame propagation. In the previous studies performed by Foong et al. [28] and Yuan et al. [4], the MFB profiles were obtained using the so-called 'reverse run model' in GT-Power. The convection multiplier of the heat transfer was varied to match the modelled pressure trace to the measured one [4,28]. Nevertheless, a good match between measured and predicted pressure traces was not easy to achieve in most cases, especially when using data from a modern multi-cylinder engine because of uncertainties surrounding measurement accuracy and trapped unburned fuel/residual gasses. It is therefore necessary to develop a better model to estimate the MFB profile, which can deal with the measurement uncertainties and, more importantly, determine the percentage of burned fuel more accurately and confidently by considering energy conservation.

The objective of this work is to investigate the impact of water injection on the combustion process using kinetic modelling. This work first models the MFB profile by solving the energy conservation equations coupled with detailed chemical kinetics. Then, the modelled MFB profile is applied in the two-zone model to simulate combustion at the critical (knock-limited) spark timing. Finally, predictive kinetic modelling is performed to quantify and analyse both the thermodynamic and chemical effects of water injection.

2. Experimental Method

The design and control of the engine used in this study are detailed in previous publications [30], so only a brief summary is provided here. The engine was derived from a Jaguar Land Rover AJ133 V8 engine, with one bank of cylinders effectively blanked off to leave an in-line four-cylinder engine. The remaining bank of cylinders was re-sleeved to reduce the total displacement to approximately 2.0 L. The specifications of the engine are listed in Table 1. As shown in Figure 1, the engine is equipped with two direct injection systems, one for fuel and one for water. A combustion air handling unit (CAHU) supplies the engine with the required airflow at a specified temperature and pressure, while a backpressure butterfly valve installed within the exhaust system controls the pressure in the exhaust manifold. The CAHU and backpressure valve (which comprise the forced induction simulator) can accurately emulate the manifold boundary conditions of any boosting system, provided the characteristics of said system are well understood. Throughout the experiments, knock-limited combustion was achieved by advancing the spark timing until the peak-to-peak amplitude of the band-pass filtered pressure traces reached a pre-defined threshold.

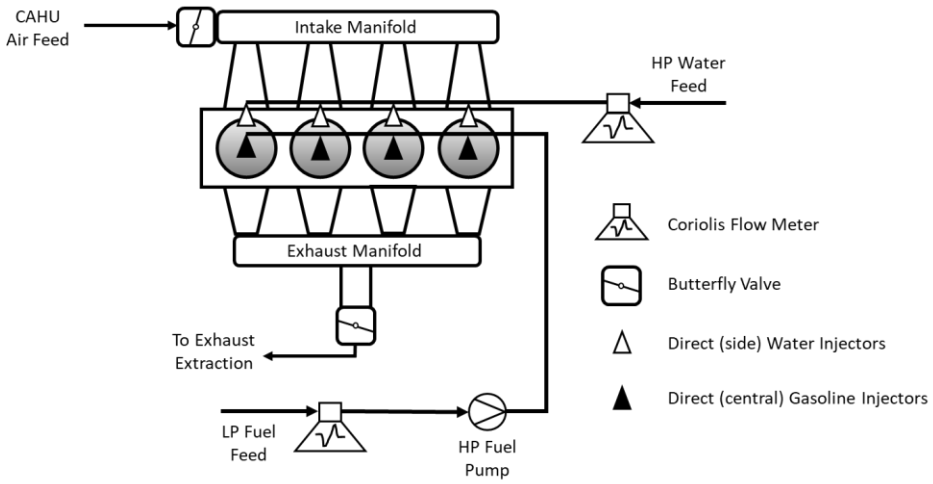

Figure 1: Schematic of general layout of test engine.

The engine was operated at 3000 rev/min with a boosted intake manifold pressure of 2.15 bar absolute. In the experiment, the fuel flow rate was around 7.0 g/s with the equivalence ratio controlled to 1.0. These operating conditions were selected to achieve a brake mean effective pressure (BMEP) of 20.5 bar. Water was injected into the cylinders at a pressure of 160 bar with an end of injection timing controlled to around 90° CA before top dead centre (TDC) firing. The controlled water injection timing represented a trade-off between maximising the charge cooling effect and maintaining acceptable combustion stability. The mass-based water/fuel ratio (WFR) was varied from 0% to 60%. With water added, the spark timing was advanced accordingly to obtain knock-limited spark advance (KLSA). The in-cylinder pressure traces under knock-limited conditions were measured using Kistler 6054A transducers with a measurement uncertainty below 0.8%, while the measurement of NOx was conducted using a Horiba MEXA 7100 DEGR exhaust gas analyser with an uncertainty below ±2%. In this study, it is assumed that NO is the main component in NOx emissions.

Table 1: Specifications of the SI engine

Engine Geometry	
Bore (mm)	83.0
Stroke (mm)	92.0
Connecting rod (mm)	148.0
Compression ratio	10.5
Number of valves	4

3. Numerical Method

Kinetic engine modelling was performed to investigate the impact of water injection on the in-cylinder combustion process. The modelling approach in this study is, in general, similar to that reported in [4] but incorporates an improved approach to obtain the MFB profile.

3.1 Gasoline surrogate

Gasoline is a complex mixture of hydrocarbons, including paraffins, aromatics, olefins, napthenes, and other additives. In kinetic modelling, gasoline is normally emulated by surrogate mixtures comprising of representative components from the aforementioned hydrocarbon groups. When formulating gasoline surrogates, priority is usually given to matching octane numbers and hydrocarbon distributions.

The gasoline used in this work is an E10 which contains 10% ethanol by volume and has a research octane number (RON) and a motor octane number (MON) of 96.8 and 86.8, respectively. The octane numbers, together with the hydrocarbon distributions are presented in Table 2. Ethanol is known to blend non-linearly with hydrocarbons in terms of octane numbers [1,31,32]. To quantify these non-linear blending behaviours, Yuan et al. [33] proposed the optimal octane number correlations for mixtures containing toluene reference fuels (TRFs) (mixtures of iso-octane, n-heptane, and toluene) and ethanol, which achieve a maximum absolute error of less than two octane numbers. The optimal octane number correlations are expressed in Eq.1 and 2, where x_1, x_2, x_3, and x_4 denote the mole fractions of iso-octane, n-heptane, toluene, and ethanol, respectively.

$$RON = 100.0x_1 + 0x_2 + 116.2x_3 + 108.0x_4 + 27.0x_1x_4 - 98.4x_2x_4(x_2 - x_4) - 9.1x_3x_4 \quad (1)$$

$$MON = 100.0x_1 + 0x_2 + 102.0x_3 + 90.7x_4 + 12.8x_1x_4 + 76.7x_2x_4 - 6.4x_3x_4 \quad (2)$$

The formulation of gasoline surrogates in this study focuses on matching RON instead of MON, as the former is commonly used to rate commercial gasolines. The volume fractions of toluene and ethanol were fixed to be 30% and 10%, respectively, in accordance with the hydrocarbon distribution of the test gasoline listed in Table 2. The

compositions of the formulated gasoline surrogate can be found in Table 3, which give the RON and MON of 97.0 and 89.4 respectively.

Table 2: The properties of gasoline used in this study

Fuel Properties	
RON	96.8
MON	86.8
Paraffins (vol%)	51.8
Aromatics (vol%)	30.3
Olefins (vol%)	8.8
Ethanol (vol%)	9.1

Table 3: Compositions of the gasoline surrogate

Fuel	vol%	mol%
iso-octane	46.0	33.6
n-heptane	14.0	11.6
toluene	30.0	34.1
ethanol	10.0	20.7

3.2 Model for combustion analysis

With the formulated gasoline surrogate, combustion analysis was performed to obtain the MFB profile which quantifies the rate at which the mixture of fuel and air is consumed by the propagating flame. The MFB profile was then used as an input for the two-zone kinetic engine model. Previous studies performed by Foong et al. [28] and Yuan et al. [4] modelled the MFB profile using the reverse run model within GT-Power. This approach tries to match the modelled pressure trace with the measured trace by scaling the overall in-cylinder heat transfer, and generates the MFB profile as an output. However, it is often difficult to get a good match between the modelled and measured pressure traces, especially on a multi-cylinder engine that is typically subject to more sources of measurement uncertainty than an equivalent single-cylinder engine.

To minimise the impact of measurement uncertainties, this study firstly identifies a representative cylinder pressure trace from the experimental data (300 consecutive cycles logged at 0.1° CA resolution). The starting point for this process involves identifying the cycle with the 95th percentile highest cylinder pressure at intake valve closure (IVC). This cycle is used as the starting point to simulate the compression process using a single-zone model and the standard Woschni heat transfer model [34]. The modelled pressure trace for compression is used as the baseline to select the measured traces with the similar compression process. Among these selected traces, the cycle with the 95th percentile most advanced combustion phasing (defined as the angle of 50% MFB) relative to all 300 measured traces, is selected as the representative pressure trace. The reason for selecting the 95th percentile most advanced trace is due to the knock-limited condition. The modelling-based selection approach is not sensitive to the uncertainties that introduce noticeable variations among different pressure traces but have limited impact on a single trace.

With the selected representative pressure trace, the approach proposed by Chun and Heywood [35] is adopted in this study to derive the MFB profile, which requires solving the energy conservation equations. In this work, detailed combustion chemistry combining the gasoline surrogate mechanism from Lawrence Livermore National Laboratory [36] and the NO sub-model from Dagaut and Nicolle [37] is incorporated into the governing equations to better estimate the thermodynamic properties of the in-cylinder gases and model the oxidation processes in both the burned and unburned gas zones. It should be noted that the comprehensive understanding of NO chemistry, especially its interactions with large hydrocarbons, is currently lacking in the literature [38,39]. Since the NO sub-model from Dagaut and Nicolle [37] worked with suitable accuracy in the modelling work performed by Yuan et al. [4], it is therefore adopted in this study too. The governing equations and initial conditions for the modelling of MFB profile (dm_x/dt) are listed in Table 4. In addition to the energy conservation equations within the cylinder, the species conservation equations in the unburned and burned gas zones are solved simultaneously. Note that these equations are based on the same assumptions made for the two-zone kinetic model in the next section. The modelling of the MFB profile starts from the spark timing and continues

until the end of combustion. The ideal gas law is used to estimate the initial mixture temperature from the measured pressure at the spark timing. It is assumed that reactions only occur after the spark timing, and the initial compositions of the unburned and burned gas zones are set to be the same as those of the fresh charge blended with residual gas at IVC. The residual gas, containing approximately 3800 ppm NO, has a mass fraction of 7.7% in the trapped gas mixture, which was determined from a validated model of the engine in GT-Power. The equations in Table 4 are solved using MATLAB with chemical kinetics handled by Cantera [40].

Table 4: Governing equations and initial conditions for the combustion analysis

Governing Equation	Initial condition
Energy conservation of the cylinder: $\left[R_b T_b - R_u T_u + \frac{R_b}{c_{p,b}}\sum_i^N Y_{i,f}\left(h_{i,f}-h_{i,b}\right) + \bar{R}T_b\sum_i^N \frac{Y_{i,f}-Y_{i,b}}{MW_{i,b}}\right]\frac{dm_x}{dt} =$ $\left(V - \frac{R_b V_b}{c_{p,b}} - \frac{R_u V_u}{c_{p,u}}\right)\frac{dp}{dt} + p\frac{dV}{dt} - \frac{R_b}{c_{p,b}}\frac{dQ_b}{dt} - \frac{R_u}{c_{p,u}}\frac{dQ_u}{dt}$ $-\bar{R}\left(V_b T_b\sum_i^N \dot{\omega}_{i,b} + V_u T_u\sum_i^N \dot{\omega}_{i,u}\right)$ $+\left(\frac{R_b V_b}{c_{p,b}}\sum_i^N h_{i,b} MW_{i,b}\dot{\omega}_{i,b} + \frac{R_u V_u}{c_{p,u}}\sum_i^N h_{i,u} MW_{i,u}\dot{\omega}_{i,u}\right)$	$m_{x,0} = 0$
Energy conservation of the unburned gas zone: $m_u c_{p,u}\frac{dT_u}{dt} = \frac{dQ_u}{dt} + V_u\frac{dp}{dt} - m_u\sum_i^N \frac{h_{i,u} MW_{i,u}\dot{\omega}_{i,u}}{\rho_u}$	$T_{u,0} = T_s = \frac{p_s V_s}{m_u R}$
Energy conservation of the burned gas zone: $m_b c_{p,b}\frac{dT_b}{dt} = \frac{dQ_b}{dt} + V_b\frac{dp}{dt} - V_b\sum_i^N h_{i,b} MW_{i,b}\dot{\omega}_{i,b} + \frac{dm_x}{dt}\sum_i^N Y_{i,f}\left(h_{i,f}-h_{i,b}\right)$	$T_{b,0} = T_{u,0}$
Mass fractions of species in the unburned gas zone: $\frac{dY_{i,u}}{dt} = \frac{MW_{i,u}\dot{\omega}_{i,u}}{\rho_u}$	$Y_{u,0}$ is the mass fractions of gas mixture containing fresh charge and residual gas, assuming no chemical reactions before spark.
Mass fractions of species in the burned gas zone: $\frac{dY_{i,b}}{dt} = \frac{MW_{i,b}\dot{\omega}_{i,b}}{\rho_b} + \frac{1}{m_b}\frac{dm_x}{dt}\left(Y_{i,f}-Y_{i,b}\right)$	$Y_{b,0} = Y_{f,0} = Y_{u,0}$ and Y_f is updated by equilibrium calculation at each time step.

The modelling approach is validated using the data from the work by Yuan et al. [4] in which the measured pressure traces are well matched by the reverse run model in GT-Power. The resulting MFB profile in [4] is first

applied to model the pressure trace which is plotted in the sub-figure in Figure 2. The modelled pressure trace is then used as the input for the combustion analysis model developed in this study, and the resulting MFB profile from our model agrees closely with the one from GT-Power, as shown in Figure 2. These results suggest that our model can be used to replace the MFB profile from GT-Power in this study.

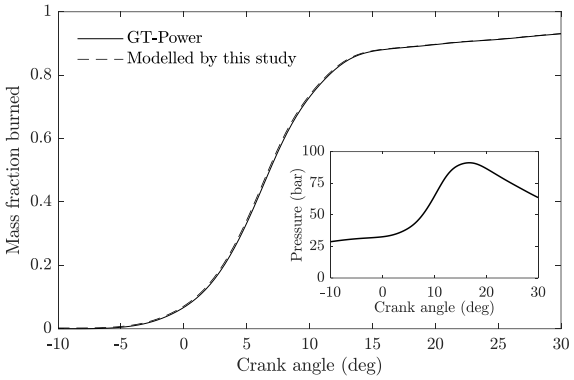

Figure 2: The comparison of the MFB profiles from GT-Power and this study.

With the proposed approach for the selection of representative pressure trace and the combustion analysis, the two-zone kinetic model can be applied to simulate combustion in modern spark ignition engines, despite their comparatively higher levels of measurement uncertainty versus single-cylinder research engines. This is a critical step to apply the fundamental knowledge of combustion chemistry to the development of high-efficiency, low-emissions spark ignition engines.

3.3 Two-zone kinetic model

The details of two-zone kinetic model have been reported by Foong et al. [28,29], and therefore only a brief summary is provided here. The modelling starts from IVC and proceeds to bottom dead centre (BDC) at the end of the expansion stroke. It therefore encompasses three stages: compression, combustion, and expansion. The compression and expansion stages are modelled with a single-zone model, and the two-zone model is used to simulate the combustion process. The flame propagation rate is dictated by the MFB profile derived using the method described earlier. The focus of the two-zone kinetic model is the prediction of autoignition in the

unburned gas zone. If autoignition occurs, the fuel in the unburned gas zone is assumed to be fully consumed by the autoignition event and the combustion modelling ends. If autoignition does not occur, the combustion modelling will continue until the end of combustion is reached and all the fuel is consumed.

The two-zone kinetic model assumes the following:

a) The gas mixtures in both unburned and burned zone are homogeneous.

b) The flame has negligible volume and allows instantaneous mass transfer and enthalpy exchange between the two zones.

c) The flame is always at chemical equilibrium.

d) The heat transfer between the two zones is negligible.

e) The remaining fuel is consumed instantaneously when the autoignition occurs.

4. Results and Discussion

In this section, results generated using the two-zone kinetic model to simulate knock-limited combustion are first presented, followed by a thermodynamic and kinetic analysis of the impact of water injection on the combustion process.

4.1 Modelling of MFB profile

With the combustion analysis model developed in this study, the measured pressure traces from this work were used to model the combustion phasing with and without water addition. In this study, the amount of water injected into the cylinder is quantified as a percentage of the injected fuel mass. A WFR value of 100% therefore represents equal mass of fuel and water being injected. During the experimental campaign, WFR was varied from 0% to 60% with an increment of 20%. Figure 3 shows the MFB profiles of the two extreme conditions, 0% and 60% WFR. Note that for the purpose of comparison, the crank angle axes of these two MFB profiles have been offset to share the same start point. It is clear that water injection leads to a slightly slower burning rate compared with

the baseline condition without water. This behaviour may be a result of the competing and contrasting effects of reduced in-cylinder temperature versus more advanced combustion phasing as WFR is increased. Since the speed of flame propagation is positively correlated to temperature, and water injection decreases the temperature of the fresh charge, it should be expected that water injection would lead to a slower flame speed and therefore a longer burn duration. Meanwhile, the reduced in-cylinder temperature allows a more advanced spark timing that increases the burning rate. Combining these two factors, the MFB profile with 60% WFR is only slightly longer than that of the baseline. The discrepancy of the two MFB profiles after entering the plateaus suggests less fresh charge is burned with 60% WFR, which is possibly due to the heterogeneous mixing and cool environment caused by the water injection. Note that these two MFB profiles plateau at values of 92%-93%, suggesting that some 7-8% of the fuel does not burn during the normal combustion process. According to the calculations performed by Cheng et al. [41], the percentage of the unburned fuel at the end of combustion process is around 9%, which agrees closely with the modelling results in this study.

Considering that water injection does not significantly affect the burn rate under the current experimental conditions, this study applies the MFB profile from the baseline condition to model the conditions with water injection. Following the modelling approach for KLSA [4], the MFB profile, as the input to the engine kinetic modelling, is shifted with the change of spark timing until the knock-limited combustion is obtained. In this case, combustion with water injection can be modelled without taking any information from the corresponding experiments, suggesting the modelling in this work is completely predictive.

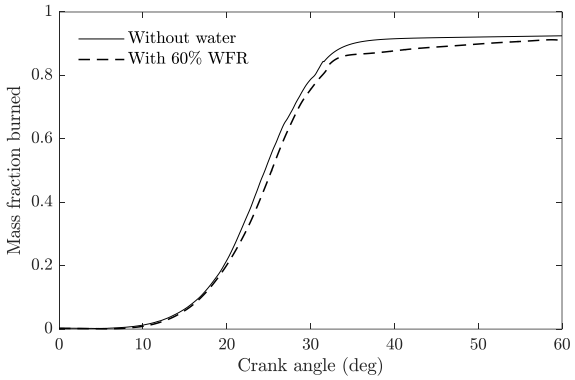

Figure 3: The comparison of the MFB profiles without and with water injection.

4.2 Modelling of the baseline

A good match between the measured and the modelled pressure trace is a prerequisite for simulating the critical spark timings at operating conditions using water injection. The MFB profile without water in Figure 3 was used as the input for the baseline modelling, and the comparison between the measurements and the modelling is shown in Figure 4. It is evident that the modelled trace agrees closely with the measurement, with small discrepancies around top dead centre (TDC) and the position of peak pressure. Note that the measured spark timing used in the modelling may not necessarily lead to knock-limited combustion.

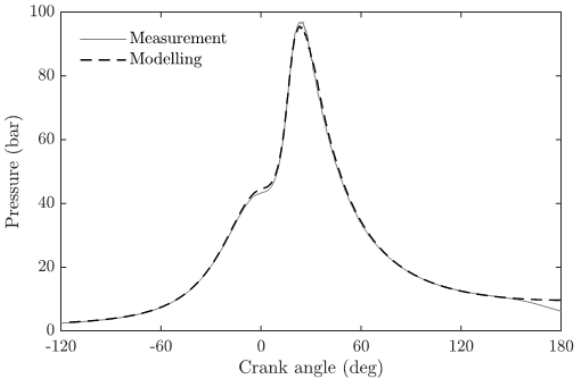

Figure 4: The comparison of measured and modelled pressure traces.

The modelling approach proposed in [4] was followed to model the critical spark timing resulting in knock-limited combustion, which assumes the combustion process lasts for 40° CAs. Figure 5(a) shows the modelled pressure traces with varied spark timings, -6.5° CA aTDC to -8.0° CA aTDC with an increment of -0.5° CA. It is apparent that a more advanced spark timing results in an earlier combustion phasing and a higher peak pressure. The critical spark timing can be identified from the corresponding unburned gas temperatures, as shown in Figure 5(b). When the spark timing is advanced to -8° CA aTDC, a sudden temperature jump is observed in the unburned gas zone near the end of combustion, indicating the occurrence of autoignition. According to these simulation results, the critical spark timing for the baseline condition is -7.5° CA aTDC since this is the most advanced spark timing that does not lead to autoignition in the unburned zone. The small discrepancy between the measured (-6.5° CA aTDC) and the modelled (-7.5° CA aTDC) knock limited spark timings suggests that the baseline operating condition is well matched by the two-zone kinetic model coupled with the detailed gasoline surrogate chemistry from LLNL [36].

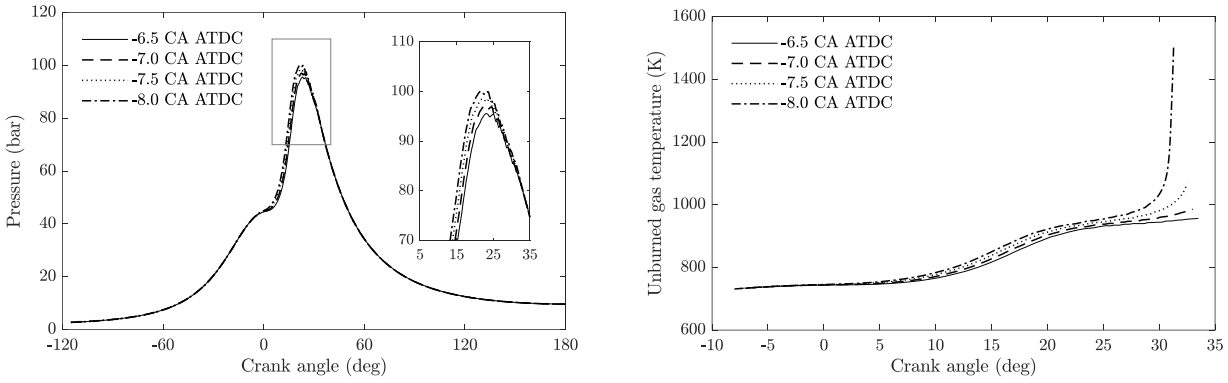

(a) (b)

Figure 5: The modelled (a) pressure traces and (b) unburned gas temperatures at different spark timings.

4.3 Modelling of water injection

With the well-matched baseline, modelling of the test conditions with water injection was performed to explore both thermodynamic and kinetic impacts of water on combustion.

4.3.1 Modelled KLSA with water injection

When water is directly injected into the cylinder, the temperature of fresh charge decreases due to the significant heat of vaporisation (HoV) of water. Considering the complicated in-cylinder heat transfer process associated with direct injection, caution is required when estimating the temperature of the fresh charge after the water injection event. To quantify the percentage of HoV that would realistically affect the temperature of the fresh charge, a separate non-kinetic GT-Power model, similar to that developed by Bozza et al. [42], was used to match the measured KLSA with water injection by varying the percentage of HoV available for charge cooling. The results of this exercise suggest that 80% of the total available HoV goes into cooling the fresh charge. It should be emphasized that the in-cylinder heat transfer process involved in the evaporation of directly injected water are very complicated and would be affected by a large number of parameters such as the amount of water injected and the injection timing. A comprehensive understanding of this process would require fundamental experiments and careful CFD simulations, both of which are beyond the scope of this work. In this study, the focus is to explore the impact of the water injection on combustion, and therefore the complex heat transfer process is approximated by a modelled, fixed fraction of HoV, which cools the fresh charge at IVC. The temperatures of the fresh charge at IVC for different WFRS (listed in Table 5) were calculated using the Ideal Gas Law.

Table 5: The estimated temperatures at IVC with different WFRs.

WFR (%)	T_{IVC} (K)
0	384.3
20	361.4
40	339.6
60	318.6

The modelled and measured critical spark timings are compared in Figure 6. As mentioned previously, the MFB profile used in the modelling with water is taken from the baseline 0% WFR condition due to the small difference between the modelled MFB profiles in Figure 3. The overall trend of the measurements is well captured

by the two-zone kinetic model, however the magnitude of the discrepancy increases as more water is injected. Although tuning the ratio of HoV used for the charge cooling helps to reduce this discrepancy, the focus of this study is to explore how combustion is affected by the water injection. Since the modelled results reproduce the experiments reasonably well, the model itself is deemed sufficiently accurate to be used in the following thermodynamic and kinetic analyses.

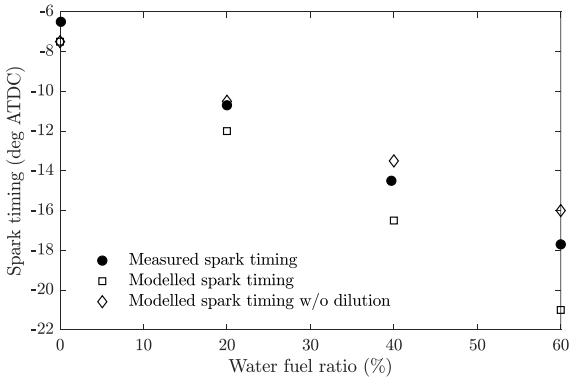

Figure 6: A comparison between the measured and the modelled critical spark timings. The modelled spark timing without dilution separates the dilution effect from the charge cooling effect.

The modelled knock-limited pressure traces and the unburned gas temperatures at 0%, 20%, 40%, and 60% WFR are compared in Figure 7. It is evident that the more advanced spark timings at higher WFRs lead to higher peak pressures. Considering an earlier spark timing also corresponds to a larger unburned gas volume at the beginning of combustion (for spark timings before TDC), a greater level of engine work ($V_u dp/dt$) compresses the unburned gas zone. This leads to a faster increase of the unburned gas temperature, especially at the incipient stage, as shown in Figure 7 (b).

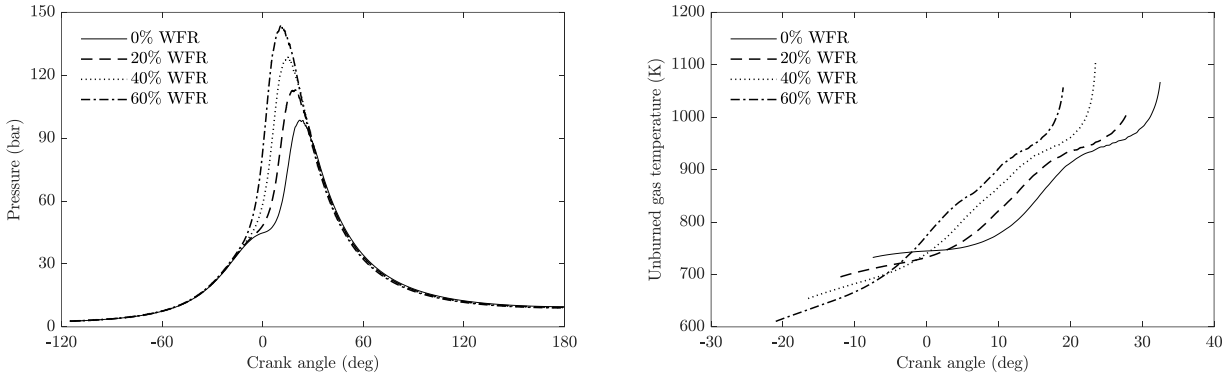

(a) (b)

Figure 7: Comparison of the modelled (a) pressure traces and (b) unburned gas temperatures with different WFRs under the KLSA condition.

4.3.2 Effects of charge cooling and dilution

Water injection not only decreases the temperature of the fresh charge, but also acts as a diluent during the compression and combustion processes. Both of these effects mitigate autoignition, enabling more advanced combustion phasing, but the quantification of these effects is sparse in the literature.

In order to isolate these effects, the temperatures at IVC listed in Table 5 were applied in the baseline (0% WFR) model, but water was not added in the modelling. Note that the pressure at IVC is fixed to the measured value, which leads to an increase in the trapped in-cylinder mass based on the ideal gas law. Therefore, this modelling approach slightly underestimates the charge cooling effect by introducing more fresh charge. The resulting critical spark timings accounting for the effect of charge cooling without water addition are included in Figure 6 under the label 'Modelled spark timing w/o dilution'. With the dilution effect eliminated, it is not surprising to find that the combustion phasing becomes less advanced, since the unburned gas temperature is higher without the dilution, leading to a stronger tendency for the end gas to autoignite. Although the dilution effect becomes more significant at higher WFRs from Figure 6, it contributes approximately one third of the total spark advance across the WFR range studied in this work. Considering the slightly increased trapped mass introduced by the fixed pressure at IVC assumption, we can conclude that the effect of charge cooling is more

significant than the modelling results indicate. Therefore, more than two thirds of the total spark advance afforded by water injection comes from the effect of charge cooling based on our estimation.

4.3.3 Kinetic analysis of water injection

The following section studies the kinetic impact of water injection on the combustion process. Given the importance of OH radicals and NO [38,39] on the oxidation process of the unburned gas zone, their predicted mole concentrations (mol/m^3) at different WFRs under the KLSA condition are compared in Figure 8. A clear trend is that higher WFRs result in higher mole concentrations of both OH radicals and NO in the unburned zone, a result of the pressure and unburned temperature profiles shown in Figure 7. Figure 8 (a) shows that at higher water fractions, the first local minimum on the OH profile, which is discernible on the curve for 0% WFR at approximately 14° CA aTDC, becomes less apparent. Comparing with the mole concentrations of NO in Figure 8 (b), it appears that for higher levels of water injection, slightly more NO is left after the initial rapid drop. This observation can be viewed more clearly in the zoomed-in plot. The increasing trend of NO at this stage in the cycle is in line with the gradually reducing first local minimum on the OH profile. According to the NO model developed by [37], NO reacts with an HO_2 radical to form NO_2 and an OH radical, which is the most significant elementary reaction leading to the initial production of OH radicals. Although NO can also react with an OH radical forming a HONO radical and slowing down the oxidation, the impact of this elementary reaction is less significant than that between NO and the HO_2 radical under the current experimental condition [39]. Therefore, the changes of NO and OH are closely related at this stage. Further kinetic analysis shows that the increasing trend of the remaining NO after the rapid drop is caused by the addition of water, which introduces other elementary reactions producing OH radical. A representative reaction among these elementary reactions is the decomposition of HONO to form OH radical and NO. Note that this decomposition reaction is a three-body reaction, and the collision partner of this reaction is actually water [37]. With the addition of water, the reaction rate of HONO decomposition increases accordingly, leading to a steady increase of OH radicals at the beginning of the combustion event. In addition, the produced

NO from the decomposition of HONO also reacts with HO_2 to form an OH radical. After this stage, the oxidation characteristics of different WFRs are similar, and most OH radicals are produced by the decompositions of oxygenated compounds originating from n-heptane and iso-octane. These decompositions are known as the chain-branching reactions in the low temperature chemistry.

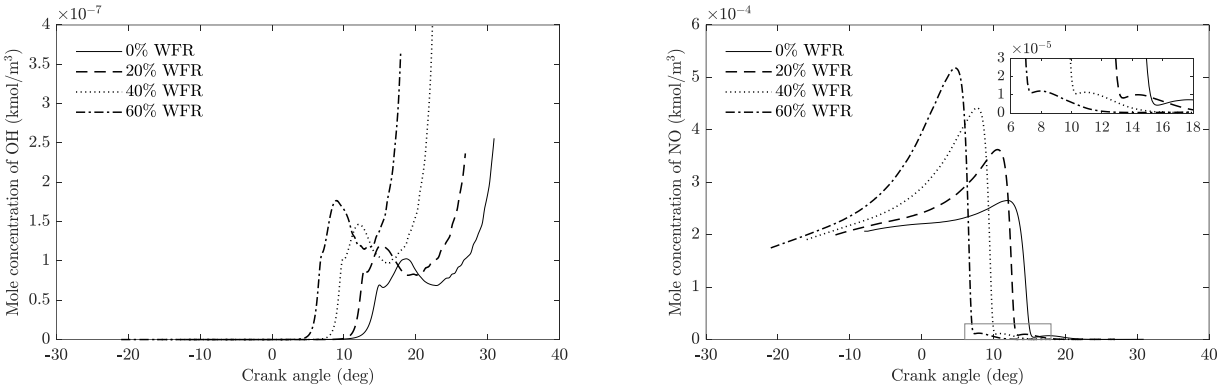

(a) (b)

Figure 8: Comparison of the mole concentrations of (a) OH and (b) NO with different WFRs under the KLSA condition.

Referring to Figure 8(a), the drops in concentration of OH radical are due to the H abstraction reactions between OH radicals and the parent fuels. Although these reactions also occur in earlier stages of oxidation, the rates of progress (ROPs) are small due to the limited amount of OH radicals available. When the initial accumulation of OH radicals is complete via both the NO chemistry and the low temperature chemistry, the oxidation of parent fuels becomes more pronounced, which is confirmed by the profiles of mole concentrations of the four parent fuels under the baseline condition, as shown in Figure 9. During the initial stages of oxidation, the mole concentrations of all parent fuels increase, indicating the fuel consumption is slower than the volume decrease of the unburned gas zone. As oxidation proceeds, the mole concentrations of the fuels start to decrease rapidly due to the H abstraction reactions by OH radicals. This decrease is consistent with the drop in concentration of OH radical between 14° CA aTDC and 24° CA aTDC shown in Figure 8(a).

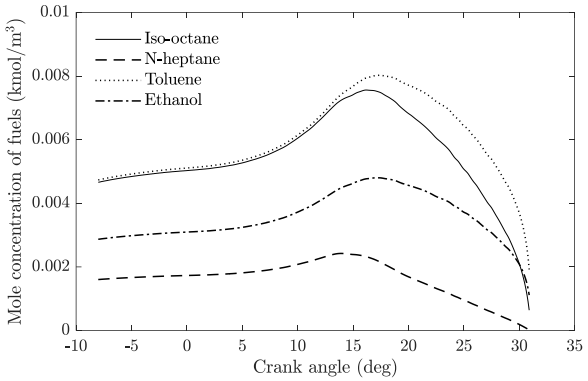

Figure 9: The mole concentrations of parent fuels in the unburned gas zone under the baseline condition.

After the second local minima in Figure 8(a), the mole concentrations of OH radical increase rapidly, leading to autoignition. At this stage, the high temperature chemistry gradually takes control of the process of oxidation. Abundant HO_2 radicals combine with each other to form H_2O_2, and the decomposition of H_2O_2 leads to a sudden jump in OH radical concentration, which increases the reactivity of the unburned gas zone significantly and causes autoignition.

Based on the kinetic analysis of OH radical in the unburned gas zone, it is clear that the addition of water changes the thermodynamic conditions inside the combustion chamber, resulting in slightly different oxidation kinetics. Note that water may also react with hydrocarbons and alter reaction pathways, especially under high temperatures, which could affect the overall reactivity [19,21,43]. In order to understand the kinetic impact of water on the autoignition chemistry as a reactant, a new species named 'H2O_inert' is added to the chemical mechanism. The new species has identical thermodynamic properties to water, but does not get involved in any elementary reactions apart from acting as a collision partner in three-body reactions. The same treatment was applied by Le Cong and Dagaut [19] and Donohoe et al. [21]. With this chemically inert species, the impact of water on the autoignition chemistry can be quantified by analysing the difference between the modelling results from the original mechanism and the modified mechanism with 'H2O_inert'. The modified mechanism was used to model the case with 60% WFR, and the resulting in-cylinder pressure and unburned gas temperature are compared with those from the original mechanism, as shown in Figure 10. The close agreement observed for both

in-cylinder pressure and unburned gas temperature indicates water has little chemical impact on the overall combustion process in SI engines under the experimental conditions in this study, which is consistent with the findings in [19,21,43]. Note that employing the modified mechanism results in unburned gas temperature predictions that are 20 K higher than that predicted by the original mechanism at the end of combustion, which is shown in the subplot of Figure 10 (b). This observation is most likely due to water acting as a reacting species in the high temperature chemistry at the end of combustion and would be expected to have a negligible impact on the oxidation process in the unburned gas zone.

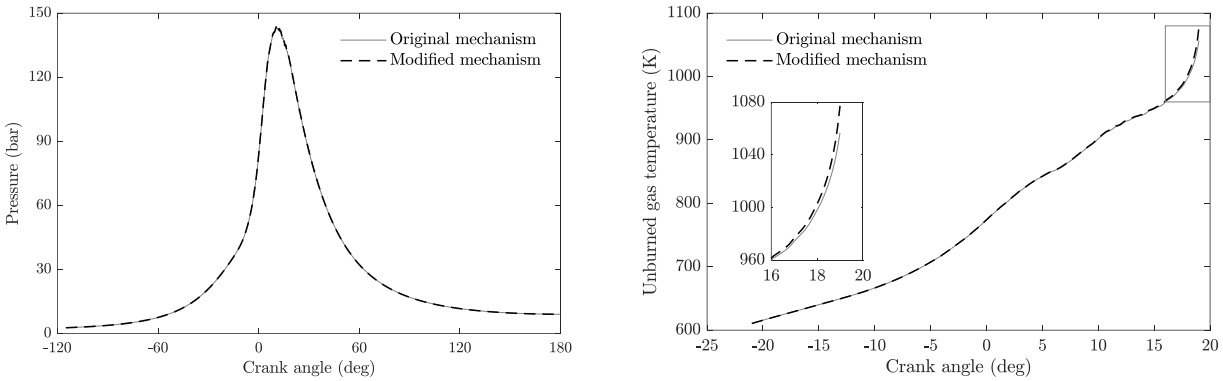

(a) (b)

Figure 10: Comparison of the modelled (a) pressure and (b) unburned gas temperature using the original and the modified chemical mechanisms.

4.3.4 Impact of water on NO emissions

Although the chemical impact of water on the autoignition of the unburned gas zone is negligible, the thermodynamic effect significantly influences the in-cylinder combustion process, which, consequently, affects the engine-out emissions of NO. Figure 11 shows that the modelled NO emissions agree reasonably well with the measurements, both showing a decreasing trend in NO with increasing WFR. Despite the significant role of NO in the oxidation of the unburned gas, the temperature of the unburned gas zone is too low to form NO, whereas the flame and the burned gas zone with temperatures above 2000 K are responsible for the formation of NO. The propagating flame, which is assumed to be at chemical equilibrium, consumes the fresh charge in the unburned

gas zone and produces small species such as NO. Meanwhile, reactions in the burned gas zone are also related to the formation of NO. The mole fractions of NO produced by the flame at different WFRs are compared in Figure 12 (a), showing that the mole fraction of NO is inversely correlated to the amount of water added.

The addition of water reduces the temperature of the unburned mixture entering the flame, which results in a lower flame temperature and, therefore, a smaller fraction of NO. In contrast, the net production rate of NO in the burned gas zone slightly increases with the addition of water, as shown in Figure 12 (b). This increase is likely due to the higher peak cylinder pressures observed at higher WFRs where combustion is more advanced. However, the small increase in the net production rate of NO in the burned gas zone is insignificant compared to the decrease in NO formation from the flame, leading to the overall decreasing trend in NO emissions shown in Figure 11.

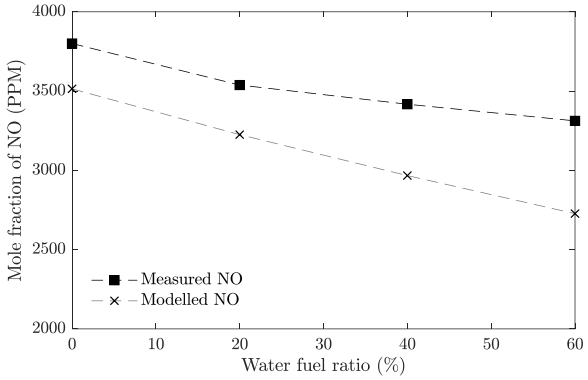

Figure 11: Measured mole fractions of NO for different WFRs at a fixed end of water injection timing of -75° CA aTDC. The modelled concentrations of NO at the end of expansion are plotted for comparison.

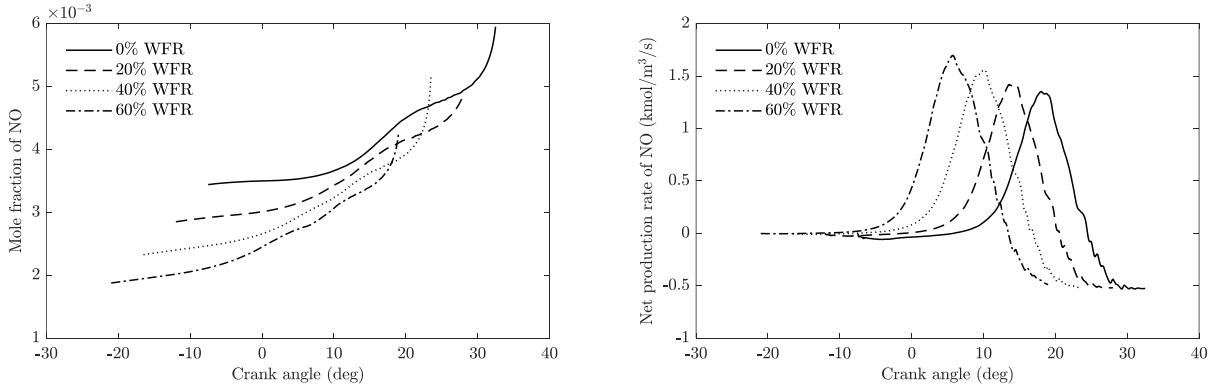

(a) (b)

Figure 12: Comparisons of (a) mole fractions of NO in the flame and (b) net production rates of NO in the burned gas zone with different WFRs.

5. Conclusion

This paper presents a numerical study on the combustion process in a modern SI engine with water injection. The modelled critical spark timings agreed well with the measurements, which validates the approach used. A comprehensive investigation of the impact of water injection on the combustion process was performed using a two-zone kinetic model. Both thermodynamic and kinetic effects of water injection were analysed based on the modelling results.

A kinetic model for combustion analysis based on measured cylinder pressure data was developed in this work. This model can be used to estimate the MFB profile and the evolution of gas temperatures and species concentrations in both the burned and unburned gas zones. The MFB profile derived for the 60% WFR condition was found to have a slightly slower burning rate than that of the 0% WFR baseline, which might be a result of the competing effects of lower in-cylinder temperatures versus more advanced combustion phasing at higher WFRs. Different WFRs ranging from 0% to 60% were modelled using the fixed MFB profile from the baseline 0% WFR condition. The modelled critical spark timings agreed reasonably well with the measurements.

Based on the modelling results, the thermodynamic effects of water injection were first investigated. The charge cooling and dilution effects were quantified by taking water out of the cylinder but maintaining the original mixture temperatures at IVC. Although the modelling approach introduces slightly more trapped mass by fixing the pressure at IVC, the overall trend is still valid, which showed that the effect of charge cooling is much more significant than the effect of dilution in terms of advancing the knock-limited combustion phasing.

The kinetic impact of water injection on the oxidation of the unburned gas zone was explored as well. It was found that the initial heat release in the unburned gas zone mainly comes from the reaction between NO and HO_2 radical. With more water injected, the first local minimum on the OH profile becomes less apparent, since the

added water acts as the collision partner to increase the ROPs of elementary reactions that produce OH radicals, (such as the decomposition reaction of HONO). This study also examined the chemical interactions between water and hydrocarbons and found that water has a negligible chemical impact on autoignition except being a collision partner. With respect to engine-out NO emissions, water injection decreases the fractions of NO at the end of combustion due to its cooling effects on the flame, the overall trend of which is well captured by the kinetic modelling.

Acknowledgements

This research was supported by Jaguar Land Rover, and the authors would like to thank Associate Professor Yi Yang from University of Melbourne for the helpful discussion on the modelling approach.

Nomenclature	
t	time (s)
T	gas temperature (K)
p	in-cylinder pressure (pa)
m	mass of gas mixture (kg)
V	volume (m^3)
Q	heat transfer into between wall and gas mixture (J)
h	mass-basis enthalpy (J/kg)
MW	molecular weight (kg/kmol)
Y	mass fraction
c_p	mass-basis specific heat at constant pressure (J/kg-K)
$\bar{R}$	universal gas constant (J/kmol-K)
R	$\bar{R}/MW$ (J/kg-K)
N	number of species
Greek letters	
ρ	density (kg/m^3)
$\dot{\omega}$	net production rate ($kmol/m^3$-s)
Subscripts	
i	species
u	unburned gas zone
b	burned gas zone
f	flame
x	mass fraction burned
0	initial condition
s	spark

Reference

[1] Foong TM, Morganti KJ, Brear MJ, da Silva G, Yang Y, Dryer FL. The octane numbers of ethanol blended with gasoline and its surrogates. Fuel 2014;115:727–739. https://doi.org/10.1016/j.fuel.2013.07.105.

[2] Foong TM, Morganti KJ, Brear MJ, da Silva G, Yang Y, Dryer FL. The Effect of Charge Cooling on the RON of Ethanol/Gasoline Blends. SAE Int J Fuels Lubr 2013;6(1):31–43. https://doi.org/10.4271/2013-01-0886.

[3] Leone TG, Anderson JE, Davis RS, Iqbal A, Reese RA, Shelby MH, et al. The Effect of Compression Ratio, Fuel Octane Rating, and Ethanol Content on Spark-Ignition Engine Efficiency. Environ Sci Technol 2015;49:10778–89. https://doi.org/10.1021/acs.est.5b01420.

[4] Yuan H, Foong TM, Chen Z, Yang Y, Brear M, Leone T, et al. Modeling of Trace Knock in a Modern SI Engine Fuelled by Ethanol/Gasoline Blends. SAE Tech Pap 2015;2015-01–1242. https://doi.org/10.4271/2015-01-1242.
[5] Zhu S, Hu B, Akehurst S, Copeland C, Lewis A, Yuan H, et al. A review of water injection applied on the internal combustion engine. Energy Convers Manag 2019;184:139–58. https://doi.org/10.1016/j.enconman.2019.01.042.
[6] Harrington JA. Water Addition to Gasoline-Effect on Combustion, Emissions, Performance, and Knock, 1982. https://doi.org/10.4271/820314.
[7] Worm J, Naber J, Duncan J, Barros S, Atkinson W. Water Injection as an Enabler for Increased Efficiency at High-Load in a Direct Injected, Boosted, SI Engine. SAE Int J Engines 2017;10. https://doi.org/10.4271/2017-01-0663.
[8] Xu P, Ji C, Wang S, Cong X, Ma Z, Tang C, et al. Effects of direct water injection on engine performance in engine fueled with hydrogen at varied excess air ratios and spark timing. Fuel 2020;269:117209. https://doi.org/10.1016/j.fuel.2020.117209.
[9] Zhuang Y, Sun Y, Huang Y, Teng Q, He B, Chen W, et al. Investigation of water injection benefits on downsized boosted direct injection spark ignition engine. Fuel 2020;264:116765. https://doi.org/10.1016/j.fuel.2019.116765.
[10] Merola SS, Irimescu A, Vaglieco BM. Influence of water injection on combustion identified through spectroscopy in an optical direct injection spark ignition engine. Fuel 2020;273:117729. https://doi.org/10.1016/j.fuel.2020.117729.
[11] Cantiani A, Viggiano A, Magi V. How to Improve SI Engine Performances by Means of Supercritical Water Injection, 2019, p. 2019-24–0235. https://doi.org/10.4271/2019-24-0235.
[12] Fan Y, Wu T, Li X, Xu M, Hung D. Influence of Port Water Injection on the Combustion Characteristics and Exhaust Emissions in a Spark-Ignition Direct-Injection Engine, 2020, p. 2020-01–0294. https://doi.org/10.4271/2020-01-0294.
[13] De Bellis V, Bozza F, Teodosio L, Valentino G. Experimental and Numerical Study of the Water Injection to Improve the Fuel Economy of a Small Size Turbocharged SI Engine. SAE Int J Engines 2017;10:550–61. https://doi.org/10.4271/2017-01-0540.
[14] Bozza F, De Bellis V, Teodosio L. Potentials of cooled EGR and water injection for knock resistance and fuel consumption improvements of gasoline engines. Appl Energy 2016;169:112–25. https://doi.org/10.1016/j.apenergy.2016.01.129.
[15] d'Adamo A, Berni F, Breda S, Lugli M, Fontanesi S, Cantore G. A Numerical Investigation on the Potentials of Water Injection as a Fuel Efficiency Enhancer in Highly Downsized GDI Engines, 2015. https://doi.org/10.4271/2015-01-0393.
[16] Senčić T, Mrzljak V, Blecich P, Bonefačić I. 2D CFD Simulation of Water Injection Strategies in a Large Marine Engine. J Mar Sci Eng 2019;7:296. https://doi.org/10.3390/jmse7090296.
[17] Zembi J, Battistoni M, Ranuzzi F, Cavina N, De Cesare M. CFD Analysis of Port Water Injection in a GDI Engine under Incipient Knock Conditions. Energies 2019;12:3409. https://doi.org/10.3390/en12183409.
[18] Yin P, Li X, Hung D, Fan Y, Xu M. Numerical Investigation of the Effects of Port Water Injection Timing on Performance and Emissions in a Gasoline Direct Injection Engine, 2020, p. 2020-01–0287. https://doi.org/10.4271/2020-01-0287.
[19] Le Cong T, Dagaut P. Experimental and Detailed Modeling Study of the Effect of Water Vapor on the Kinetics of Combustion of Hydrogen and Natural Gas, Impact on NOx. Energy Fuels 2009;23:725–34. https://doi.org/10.1021/ef800832q.

588 [20] Schmitt S, Wick M, Wouters C, Ruwe L, Graf I, Andert J, et al. Effects of water addition on the
589 combustion of iso-octane investigated in laminar flames, low-temperature reactors, and an HCCI
590 engine. Combust Flame 2020;212:433–47. https://doi.org/10.1016/j.combustflame.2019.11.023.
591 [21] Donohoe N, Heufer KA, Aul CJ, Petersen EL, Bourque G, Gordon R, et al. Influence of steam
592 dilution on the ignition of hydrogen, syngas and natural gas blends at elevated pressures. Combust
593 Flame 2015;162:1126–35. https://doi.org/10.1016/j.combustflame.2014.10.005.
594 [22] He X, Donovan MT, Zigler BT, Palmer TR, Walton SM, Wooldridge MS, et al. An experimental
595 and modeling study of iso-octane ignition delay times under homogeneous charge compression
596 ignition conditions. Combust Flame 2005;142:266–75.
597 https://doi.org/10.1016/j.combustflame.2005.02.014.
598 [23] Szybist JP, Splitter DA. Pressure and temperature effects on fuels with varying octane sensitivity at
599 high load in SI engines. Combust Flame 2017;177:49–66.
600 https://doi.org/10.1016/j.combustflame.2016.12.002.
601 [24] Agbro E, Tomlin AS, Zhang W, Burluka A, Mauss F, Pasternak M, et al. Chemical Kinetic
602 Modelling Study on the Influence of n-butanol blending on the Combustion, Autoignition and
603 Knock Properties of Gasoline and its Surrogate in a Spark Ignition Engine. Energy Fuels 2018.
604 https://doi.org/10.1021/acs.energyfuels.8b00962.
605 [25] Gamma Technologies. GT-Power user's manual, version 7.3. 2012.
606 [26] Morganti KJ, Brear MJ, da Silva G, Yang Y, Dryer FL. The autoignition of Liquefied Petroleum
607 Gas (LPG) in spark-ignition engines. Proc Combust Inst 2014.
608 https://doi.org/10.1016/j.proci.2014.06.070.
609 [27] DelVescovo DA, Splitter DA, Szybist JP, Jatana GS. Modeling pre-spark heat release and low
610 temperature chemistry of iso-octane in a boosted spark-ignition engine. Combust Flame
611 2020;212:39–52. https://doi.org/10.1016/j.combustflame.2019.10.009.
612 [28] Foong TM, Brear MJ, Morganti KJ, da Silva G, Yang Y, Dryer FL. Modeling End-Gas
613 Autoignition of Ethanol/Gasoline Surrogate Blends in the Cooperative Fuel Research Engine.
614 Energy Fuels 2017;31:2378–89. https://doi.org/10.1021/acs.energyfuels.6b02380.
615 [29] Foong TM. On the Autoignition of Ethanol/Gasoline Blends in Spark-Ignition Engines. Ph.D.
616 Thesis. The University of Melbourne, 2013.
617 [30] Turner JWG, Popplewell A, Patel R, Johnson TR, Darnton NJ, Richardson S, et al. Ultra Boost for
618 Economy: Extending the Limits of Extreme Engine Downsizing. SAE Int J Engines 2014;7:387–
619 417.
620 [31] Badra J, AlRamadan AS, Sarathy SM. Optimization of the octane response of gasoline/ethanol
621 blends. Appl Energy 2017;203:778–793. https://doi.org/10.1016/j.apenergy.2017.06.084.
622 [32] Yuan H, Chen Z, Zhou Z, Yang Y, Brear MJ, Anderson JE. Formulating gasoline surrogate for
623 emulating octane blending properties with ethanol. Fuel 2020;261:116243.
624 https://doi.org/10.1016/j.fuel.2019.116243.
625 [33] Yuan H, Yang Y, Brear MJ, Foong TM, Anderson JE. Optimal octane number correlations for
626 mixtures of toluene reference fuels (TRFs) and ethanol. Fuel 2017;188:408–17.
627 https://doi.org/10.1016/j.fuel.2016.10.042.
628 [34] Woschni G. A Universally Applicable Equation for the Instantaneous Heat Transfer Coefficient in
629 the Internal Combustion Engine. SAE Tech Pap 1967;670931. https://doi.org/10.4271/670931.
630 [35] Chun KM, Heywood JB. Estimating Heat-Release and Mass-of-Mixture Burned from Spark-
631 Ignition Engine Pressure Data. Combust Sci Technol 1987;54:133–43.
632 https://doi.org/10.1080/00102208708947049.

[36] Mehl M, Pitz WJ, Westbrook CK, Curran HJ. Kinetic modeling of gasoline surrogate components and mixtures under engine conditions. Proc Combust Inst 2011;33:193–200. https://doi.org/10.1016/j.proci.2010.05.027.
[37] Dagaut P, Nicolle A. Experimental study and detailed kinetic modeling of the effect of exhaust gas on fuel combustion: mutual sensitization of the oxidation of nitric oxide and methane over extended temperature and pressure ranges. Combust Flame 2005;140:161–171. https://doi.org/10.1016/j.combustflame.2004.11.003.
[38] Chen Z, Zhang P, Yang Y, Brear MJ, He X, Wang Z. Impact of nitric oxide (NO) on n-heptane autoignition in a rapid compression machine. Combust Flame 2017;186:94–104. https://doi.org/10.1016/j.combustflame.2017.07.036.
[39] Chen Z, Yuan H, Foong TM, Yang Y, Brear M. The impact of nitric oxide on knock in the octane rating engine. Fuel 2019;235:495–503. https://doi.org/10.1016/j.fuel.2018.08.039.
[40] Goodwin DG, Moffat HK, Speth RL. Cantera: An Object-oriented Software Toolkit for Chemical Kinetics, Thermodynamics, and Transport Processes. 2016.
[41] Cheng WK, Hamrin D, Heywood JB, Hochgreb S, Min K, Norris M. An Overview of Hydrocarbon Emissions Mechanisms in Spark-Ignition Engines, 1993, p. 932708. https://doi.org/10.4271/932708.
[42] Bozza F, De Bellis V, Giannattasio P, Teodosio L, Marchitto L. Extension and Validation of a 1D Model Applied to the Analysis of a Water Injected Turbocharged Spark Ignited Engine at High Loads and over a WLTP Driving Cycle. SAE Int J Engines 2017;10:2141–53.